

Evidence of Sub-proton-scale Magnetic Holes in the Venusian Magnetosheath

Katherine A. Goodrich¹, John W. Bonnell¹, Shannon Curry¹, Roberto Livi¹,
Phyllis Whittlesey¹, Forrest Mozer^{1,2}, David Malaspina³, Jasper Halekas⁴,
Michael McManus^{1,2}, Stuart Bale^{1,2}, Trevor Bowen¹, Anthony Case⁵, Thierry
Dudok de Wit⁶, Keith Goetz⁷, Peter Harvey¹, Justin Kasper⁸, Davin Larson¹,
Robert MacDowall⁹, Marc Pulupa¹, Michael Stevens⁵

¹Space Sciences Laboratory, University of California, Berkeley, CA 94720-7450, USA

²Physics Department, University of California, Berkeley, CA 94720-7300, USA

³University of Colorado at Boulder, Boulder, CO, USA

⁴Department of Physics and Astronomy, University of Iowa, Iowa City, IA, USA

⁵Harvard-Smithsonian Center for Astrophysics, Cambridge, MA, USA

⁶University of Orléans, Orléans, France

⁷University of Minnesota, Minneapolis, MN, USA

⁸University of Michigan, Anna Arbor, MI, USA

⁹NASA, Goddard Space Flight Center, Greenbelt, MD, USA

Key Points:

- Magnetic depressions with spatial scales less than the local proton gyroradius are observed in the Venusian magnetosheath.
- Electric field associated with these depressions are consistent with electron current vortex structures.
- Similar structures have been observed in the terrestrial magnetosphere, suggesting they are part of a universal plasma process.

Abstract

Depressions in magnetic field strength, commonly referred to as magnetic holes, are observed ubiquitously in space plasmas. Sub-proton-scale magnetic holes with spatial scales smaller than or on the order of ρ_p , are likely supported by electron current vortices, rotating perpendicular to the ambient magnetic field. While there are numerous accounts of sub-proton-scale magnetic holes within the Earth's magnetosphere, there are no reported observations in other space plasma environments. We present the first evidence of sub-proton-scale magnetic holes in the Venusian magnetosheath. During Parker Solar Probe's first Venus Gravity Assist, the spacecraft crossed the planet's bow shock and subsequently observed the Venusian magnetosheath. The FIELDS instrument suite on-board the spacecraft achieved magnetic and electric field measurements of magnetic hole structures. The electric field associated with magnetic depressions are consistent with electron current vortices with amplitudes on the order of $1 \mu\text{A}/\text{m}^2$.

Plain Language Summary

The Sun is constantly ejecting an ionized gas, or plasma. This plasma from this Sun is called the solar wind and usually consists of an equal number of negatively charged electrons and their larger positively charged counterparts, protons. These particles travel together from the Sun, cancelling out each other's charge. When the plasma encounters obstacles, however, like the Earth or Venus, the plasma becomes disturbed. This can cause the electrons can separate from the protons and form unbalanced structures. One interesting structure that has recently been discovered at Earth are electron vortices. These vortices can create their own magnetic and electric fields and slightly alter the plasma around them. We have seen electron vortices where the solar wind meets the Earth, but are not sure how they are created or how strongly they affect the plasma around them. We report, for the first time, evidence of electron vortices where the solar wind encounters Venus. These new findings show the process that creates electron vortices takes place at both Earth and Venus, strongly implying a universal process in space.

1 Introduction

Sub-proton-scale magnetic holes are depressions in total magnetic field (\mathbf{B}) strength with spatial scales less than, or on the order of, a proton gyroradius (ρ_p). Depressions in $|\mathbf{B}|$ that are spatially larger than ρ_p can usually be attributed to the magnetic mir-

ror instability (Southwood & Kivelson, 1993), so much so they are commonly referred to as mirror mode waves. Mirror mode waves have been observed frequently in multiple space plasma environments such as the solar wind (Wintertialter et al., 1994; Russell et al., 2008) and terrestrial magnetosheath (Johnson & Cheng, 1997; Soucek et al., 2008). They are generally known to be generated via a plasma temperature anisotropy (Califano et al., 2008; Kuznetsov et al., 2008).

Sub-proton-scale magnetic holes are measured to be less than or on the order of the local proton gyroradius, and therefore cannot be explained by the mirror instability. Also, unlike mirror-wave modes, sub-proton-scale magnetic holes are observed with features consistent with current layers carried by electrons (Gershman et al., 2016; Goodrich, Ergun, & Stawarz, 2016). While the structure may extend longer than a ρ_p (Goodrich, Ergun, & Stawarz, 2016)), the current layers associated with sub-proton-scale magnetic holes have spatial scales smaller than ρ_p . Sub-proton-scale magnetic holes have been observed within the Earth's magnetosphere during times of magnetic field fluctuations, particularly in the magnetosheath (Huang et al., 2017; Liu et al., 2019; Yao et al., 2017) and near-Earth plasmashet (Ge et al., 2011; Sun et al., 2012; Tenerani et al., 2012, 2013; Sundberg et al., 2015; Gershman et al., 2016). Currents carried by such electron vortices have been observed both through high resolution particle measurements from the Magnetospheric Multiscale (MMS) mission (Gershman et al., 2016) as well as electric field measurements (Goodrich, Ergun, Wilder, et al., 2016a) from both MMS and THEMIS (Goodrich, Ergun, & Stawarz, 2016).

Sub-proton-scale magnetic holes are often thought to arise through a the nonlinear evolution the mirror instability and the tearing instability (Ahmadi et al., 2017; Balikhin et al., 2010, 2012). This has not been observationally confirmed. Additionally, the simulations performed by Haynes et al. (2015) and Roytershteyn et al. (2015) suggest sub-proton-scale magnetic holes arise as a coherent structure in plasma turbulence. The spatial size of sub-proton-scale magnetic holes ($< \rho_p$), however, excludes them from the mirror instability. The tearing instability is also insufficient to explain these structures as the required shear in perpendicular magnetic field components has not been observed.

While observations of sub-proton-scale magnetic holes have become increasingly frequent in recent years, their role and importance to space plasma physics is not well known. Confirmed reports of sub-proton-scale magnetic holes in both the terrestrial mag-

netosheath and plasmasheet suggest they may be a product of a universal process. However, there are currently no observations of such signatures that extend beyond the terrestrial magnetosphere. This is likely due to the fact that structures with this spatial scale is difficult to observe given the time resolution limitations on particle instruments available on previous missions to Venus, Mercury, and Mars. Additionally, the majority of these missions do not possess a full range of electric field observations, which can also be used to observe electron currents.

We report, for the first time, evidence of structures bearing significant similarities to sub-proton-scale magnetic holes in the Venusian magnetosheath. These structures were observed by the Parker Solar Probe (PSP) spacecraft during its initial Venus Gravity Assist (VGA1). Significant depressions in magnetic field strength (up to 30% of the original $|\mathbf{B}|$ value) were observed at length scales less than the local thermal proton gyroradius throughout the Venusian magnetosheath. These magnetic depressions have corresponding unipolar and bipolar electric field signals that are consistent with the presence of electron vortices.

In this paper, we review the observations from VGA1, and the magnetic hole structures found within. We then compare these observations with a simple model of an electron vortex. This comparison shows the observed signatures are largely consistent with electron vortices. These observations bear strong similarities to sub-proton-scale magnetic holes observed in the terrestrial magnetosphere. This report suggests these structures are indicative of a universal, or pervasive, process in magnetospheric plasmas.

2 Data and Instruments

The measurements examined in this study are taken from the Parker Solar Probe mission (Fox et al., 2016). Its purpose is to measure the young solar wind by obtaining measurements as close as nine solar radii from the surface of the Sun. In order for the spacecraft to reach this destination, it must encounter Venus seven times for gravitational assistance. Here we examine fields and particle measurements taken during the first Venus gravity assist, heretofore referred to as VGA1, on October 3rd, 2018 between 07:00 and 08:50 UTC.

Observations of electric field and magnetic field were obtained via the FIELDS instrument suite (Bale et al., 2016; Malaspina et al., 2016). This suite measures magnetic

field from two fluxgate magnetometers (FGM) as well as a search coil magnetometer (SCM), all of which are mounted on the magnetometer boom directly behind the heat shield. Four 2 m antennas, which measure electric potentials V_1 , V_2 , V_3 , and V_4 , are positioned in the plane of the heat shield, perpendicular to the sun-spacecraft direction. The fifth potential, V_5 , is measured by a 21 cm antenna, also mounted on the magnetometer boom. The electric field in the plane of the heat shield is derived from the differential voltage measurements ($V_1 - V_2$ and $V_3 - V_4$) calculated on the spacecraft.

The electric fields were calibrated by least squares fitting twelve second averages of E_X versus $-(v_i \times \mathbf{B})_X$ and E_Y versus $-(v_i \times \mathbf{B})_Y$, where v_i is the proton velocity from SPC. The four least squares coefficients were two dc offsets resulting from electronic offsets, the effective antenna length, and an angular rotation of the fields in the X-Y plane. This rotation was found necessary and may have resulted because the electric field antenna was comparable in size to the spacecraft and the Debye length, as described further in **Mozer et al., (2020, submitted)**.

All particle measurements used in this analysis were provided by the Solar Wind Electrons Alphas and Protons (SWEAP) instrument suite (Kasper et al., 2016). Electron moments and distributions were measured by the SPAN-electron instrument (Halekas et al., 2020; Whittlesey et al., 2020). Ion moments and distributions were measured by the Solar Probe Cup (SPC) (Case et al., 2020) and SPAN-ion (Kasper et al., 2016) instruments. SPC has a 40° half-angle field of view, with its center pointed directly sunward. SPAN-ion has a $120^\circ \times 247.5^\circ$ view of the sky perpendicular to the sunward direction. The combination of SPC and SPAN-ion provides a nearly full view of the sky. During VGA1, SPC had a 1.3 second temporal resolution. SPAN-electron and SPAN-ion had a temporal cadence of ~ 28 seconds.

A detailed description of the first Parker Solar Probe Venus Gravity Assist as well as its implications are reported by **Curry et al., [2020] (this issue)**. Figure 1 shows an overview of VGA1, which displays magnetic field, proton density (n_p), proton velocity (\mathbf{V}_p), electron energy flux, ion energy flux from SPAN-ion, and high pass filtered electric field (all signal below 1 Hz removed), in descending order. All vectors are shown in the spacecraft frame, where Z is pointed sunward and X is pointed along the spacecraft trajectory in the plane of the heat shield. It is of note that these measurements are the first ever current-biased DC electric field measurements at Venus.

All proton measurements examined are taken from SPC unless otherwise stated. For all \mathbf{V}_p , n_p , and temperature (T_p , not displayed) moments, the times at which $n_p = 0$ were removed. All data were subsequently median smoothed over eleven consecutive point intervals. The focus of this study are structures with spatial scales less than ρ_p , which are observed over tens of milliseconds. This time frame is well below the time resolution of all available particle instruments and therefore this treatment of the particle data is appropriate to provide overall context of the plasma environment during VGA1.

The PSP spacecraft made its approach traveling in the sunward direction and encountered the Venusian environment on its dawnward-flank side. Between 7:00 and 8:00 UTC, the spacecraft detected solar wind plasma. This is evident from steady proton density and antisunward velocity at 10 cm^{-3} and 450 km/s respectively. There are no coherent features observed by SPAN-ion and the magnetic field remains at a constant amplitude of $\sim 5 \text{ nT}$. The spacecraft subsequently (between 8:00 and 8:22 UTC) observes magnetic fluctuations and broad energy signals in ion energy flux from SPAN-ion. This indicates ion flows outside of the SPC field of view, which is consistent with the presence of reflected ions from the Venusian bow shock.

PSP likely crossed the Venusian bow shock and entered the magnetosheath for the first time at $\sim 08:22:20 \text{ UTC}$. This is indicated by the abrupt increase in $|\mathbf{B}|$ and n_p , as well as a deviation in proton velocity. The spacecraft subsequently crossed the bow shock approximately five times before it approached the magnetic pile-up region at 8:50 UTC. At this time all instruments were powered off due to a solar limb sensor anomaly, and no further data were collected during the encounter.

The vertical lines in Figure 1 highlight times in which sub-proton-scale magnetic hole candidates were observed. Eleven candidates were identified after the initial bow shock crossing in the Venusian magnetosheath. These structures were identified by a distinct decrease in $|\mathbf{B}|$, as well as corresponding \mathbf{E} field signatures, with observation times over tens of milliseconds. The candidates identified showed no overall change in the average (over one second) magnetic field. They were also observed alongside electric field signatures that will be discussed in depth in the following sections of this paper. All candidates were found within the Venusian magnetosheath. No magnetic holes were observed in the solar wind or foreshock regions prior to observing the initial shock crossing, sug-

gesting they are generated through a process that takes place within the Venusian magnetosheath.

3 Magnetic Hole Observations

Figure 2 shows an example of two magnetic hole candidates. It shows a 1.5 second zoomed in view of the magnetic field, electric field and proton velocity at $\sim 8:22:52$ UTC, ~ 30 seconds after the spacecraft's initial encounter with the Venusian bow shock. All vectors are shown in the spacecraft frame. E_x and E_y are directly measured by the four voltage probes in the plane aligned with the heat shield. E_z is calculated under the assumption that $\mathbf{E} \cdot \mathbf{B} = 0$. This assumption is appropriate as all observed electric field associated with sub-proton-scale magnetic holes have been primarily perpendicular to the magnetic field (Goodrich, Ergun, Wilder, et al., 2016b, 2016a).

The observed $\Delta|\mathbf{B}|/|\mathbf{B}|$ for each event is $\sim 35\%$ ($\sim 5/14$ nT) and the magnetic field direction shows little deviation ($\sim 2^\circ$) from the surrounding magnetic field. Both events are observed over 50 ms. The spatial length of the structure can be found under the assumption that it is stationary in the plasma (i.e. solar wind proton) frame. Sub-proton-scale magnetic holes have been shown to travel with the plasma by Liu et al. (2019). The spatial length of the magnetic holes are estimated to be 20 km, as the protons are measured to travel ~ 400 km/s anti-sunward. This scale falls within the sub-proton-scale as the estimated proton gyroradius in this region is 40 km ($\sqrt{m_p T_p / B^2}$, derived via observations from the flux gate magnetometer and proton temperature moments from SPC). These characteristics are all consistent with prior observations of sub-proton-scale magnetic holes in the terrestrial context.

Electric field signals are seen in conjunction with the observed magnetic field depressions. A unipolar pulse reaching ~ 10 mV/m and ~ 20 mV/m is seen in the Y and Z directions respectively. A bipolar signal with an amplitude of ~ 10 mV/m is seen in the X direction. These signatures are qualitatively consistent with sub-proton-scale magnetic holes observed in the Earth's magnetosphere. These signals bear similarities to electrostatic solitary waves like electron phase-space holes (EHs) and ion phase-space holes (IHs) (Ergun et al., 1998). It is, however, very unlikely that these signatures can be identified as either. These structures are expected to travel at the electron and proton thermal speeds (v_{Te} , v_{Tp}) respectively (Ergun et al., 1998) and have spatial scales on the or-

der of 10s (EHs) to 100s (IHs) of Debye lengths (λ_D). Electron temperatures in the magnetosheath are measured to be on the order of 40 eV (from the method described in Halekas et al. (2020)), which corresponds to a v_{Te} of 3750 km/s. This yields a scale size of 188 km for a structure observed over 50 ms in the Venusian magnetosheath. This is 18800 times greater than λ_D , estimated to be 10 m.

The electric fields in Figure 2 may be more consistent with IHs, which have an estimated to have a scale size of 3.25 km (over 50 ms, given a proton temperature of 22 eV measured from SPC). It is possible for IHs to produce a magnetic signal under a Lorentz transformation from the IH frame to the spacecraft frame. However, under the Lorentz transformation, an IH traveling at v_{Tp} produces a change in $|\mathbf{B}|$ of 0.2 fT. In order to produce the observed decrease in $|\mathbf{B}|$ (~ 5 nT), an IH with an E field amplitude of 20 mV/m must have a relative velocity of 2×10^6 km/s, $2/3$ the speed of light.

Given the above parameters, it is far more likely that the observed magnetic depressions are caused by diamagnetic electron currents, rather than electrostatic solitary waves. It is of note that there are many observed solitary waves in the Venusian magnetosheath with no magnetic field depletions. These waves may correspond to sub-proton-scale magnetic holes under different conditions. They may also correspond to electrostatic solitary waves, dust impacts or other unexplored phenomena. This paper, however, focuses on the electric field signatures with observable magnetic field depletions.

4 Model

In order to interpret these observations, we propose of a model of a sub-proton-scale magnetic hole and compare it's magnetic and electric field structures to the observed features. We construct a cylindrically symmetric current vortex. The current in this model is carried solely by electrons and is stationary in the plasma frame. The current J_ϕ is defined as

$$J_\phi = \begin{cases} J_0 \sin\left(\frac{\pi r}{2R}\right) & \text{if } r \leq R \\ 0 & \text{if } r > R \end{cases} \quad (1)$$

where r is the radial distance from the center of the magnetic hole and R is the estimated radius of the magnetic hole structure. J_0 is the maximum current density within the structure. We then simulated a spacecraft crossing this structure in various trajectories.

Multiple trajectories and values of J_0 and R were tested with this model. All trajectories were parallel to the along-track direction, while the offset distance from the center of the structure in the cross-track direction varied. The trajectory is assumed to be perpendicular to the axis of symmetry of the vortex. The magnetic and electric field induced by the vortex were then calculated based on the defined spacecraft trajectory.

The induced magnetic field from this current is derived using Amperes law,

$$\Delta \mathbf{B}_{\mathbf{Z}}(r_{SC}) = \frac{\mu_0}{R} \int_{r_{SC}}^R J_{\phi}(r) r dr. \quad (2)$$

The resulting magnetic field then becomes $\mathbf{B}_{\mathbf{Z}}(r_{SC}) = \mathbf{B}_{\mathbf{Z}}(R) - \Delta \mathbf{B}_{\mathbf{Z}}(r_{SC})$, where r_{SC} is the radial position of the simulated spacecraft. The electric field was derived via the Lorentz equation (Stix, 1992),

$$\mathbf{E}_{\mathbf{R}}(x_{SC}, y_{SC}) = -\mathbf{v}_{\mathbf{e}}(x_{SC}, y_{SC}) \times \mathbf{B}_{\mathbf{Z}}(r_{SC}). \quad (3)$$

The electron velocity as a function of spacecraft position ($\mathbf{v}_{\mathbf{e}}(x_{SC}, y_{SC})$) was determined by $\mathbf{v}_{\mathbf{e}} = -J_{\phi}(r_{SC})/qn_e$. $\mathbf{v}_{\mathbf{e}}$ is estimated to be on the order of 2000 km/s, calculated from $\mathbf{E} \times \mathbf{B}$ measurements from PSP. The density of the current layer, n_e , can therefore be estimated by $J_0/q\mathbf{E}_{\mathbf{R}} \times \mathbf{B}_{\mathbf{Z}}$. This calculation is expected to be less than the measured proton density n_p measured by SPC ($\sim 30 \text{ cm}^{-3}$).

The parameters of the model, particularly the radius of the structure (R), current density amplitude (J_0), and offset of the trajectory from the center of the vortex were all varied to best replicate the characteristics of the second magnetic hole candidate in Figure 2. Under the assumption that the structure is stationary in the plasma frame R must be on the order of $V_{SPC}\Delta t/2$ (10 km). J_0 was chosen such that the induced magnetic field produced the same $\Delta|\mathbf{B}|$ observed by PSP ($\sim 5 \text{ nT}$).

We found the following values to be consistent with the chosen example:

- $R = 15 \text{ km}$
- $J_0 = 1.75 \text{ } \mu\text{A/m}^2$
- Offset = 9 km
- $n_e = 5.5 \text{ cm}^{-3}$

Figure 3 shows a direct comparison between the observed magnetic and electric field of the sub-proton-scale magnetic hole (b and d) and those derived by the model (a and c) with the listed parameters. The observed $\mathbf{E}_{\mathbf{R}}$ and $\mathbf{B}_{\mathbf{Z}}$ vectors in this figure were rotated

into the plasma frame where the red vector ("B") is aligned with the magnetic field. The blue vector ("along") signifies the proton flow direction (perpendicular to the magnetic field), this is analogous to the "along-track" direction. The green vector ("cross") is aligned in the "cross-track" direction.

The modeled magnetic field decreases by 5.3 nT, matching the observed $\Delta|\mathbf{B}|$ observed by PSP (5.2 nT). This overall decrease is observed over 23 km in the model, which is further consistent with the observation time of the structure (~ 20 km). The modeled electric fields also bear certain similarities to observations. Firstly, the amplitudes of the modeled electric field (~ 9.75 and 16 mV/m for along and cross track respectively) are consistent with those observed (~ 25 and ~ 8 mV/m). The ratio of these amplitudes is approximately $1/2$ in the model and $1/3$ in observations, suggesting the modeled trajectory offset is consistent with the trajectory of the PSP spacecraft.

The electric fields derived from the model, however, deviate in direction from the observations by $\sim 90^\circ$. It is unclear, at this time, what the reason is for this deviation. One likely source of error may be contamination from a plasma wake from the spacecraft. Another source of error may be that the full plasma flow in the Venusian magnetosheath may lie partially outside of the field of view of the SPC and SPAN-ion instruments. All of the above may influence our analysis.

5 Discussion

In the previous section, we constructed an electron current vortex model with the intention of recreating observations from the Parker Solar Probe in the Venusian magnetosheath. This model is consistent with most of the characteristics of observed sub-proton-scale magnetic holes. The current vortex model matches the estimated size of the observed magnetic hole. The induced a magnetic field from the model is also consistent (within 2%) with the $\Delta|\mathbf{B}|$ observed by PSP. The model also produced electric fields with amplitudes similar to those observed (on the order of 10 mV/m, within 35%). The electric fields induced in the model, however, does not match the orientation of the fields seen in the observations. In fact, the observed electric fields deviate $\sim 90^\circ$ from the model.

The electric fields from all other magnetic hole candidates were also rotated in the plasma frame. All candidates deviated close to 90° in the azimuthal direction from the

model, in addition to the candidate in Figure 3. This suggests the deviation is related to a systematic or instrumental issue, rather than an issue from the plasma itself.

Contamination from a plasma wake is likely to contribute the most significant error in this case. The electric field instrument consists of four single voltage probes, V1, V2, V3 and V4. Two-dimensional electric field are constructed by taking the potential difference between two pairs V1 - V2 (dV12) and V3 - V4 (dV34). These probe pairs are nearly, but not fully, orthogonal. V3 is oriented 40° from the anti-ram direction of the spacecraft while V2 deviate 55° . As such, V3 lies more parallel to the heat shield in the anti-ram direction and thus more likely to be contaminated by the potentials due to the spacecraft's plasma wake.

During VGA1, V3 measured an electric potential that differed significantly from V1, V2, and V4. In the Venusian magnetosheath, the average electric potential between V1 and V2 differs up to 50 mV. The potential difference between V3 and V4 is approximately 130 mV, almost 3 times greater. The potential difference between V3 and V4 is even higher in the solar wind observed prior to the initial shock crossing, ~ 240 mV (6 times greater than V1 - V2).

Such a large deviation in potential suggests that V3 experiences plasma and potential conditions that are significantly different from those seen on V1, V2 and V4. The fact that this deviation changes when crossing from the solar wind into the Venusian magnetosheath suggests the effect is dependent on overall plasma conditions. Both of these points are consistent with the effects of a plasma wake.

At this time, it is unclear the what the exact contribution of this possible wake effect is on electric potential and field measurements. Contamination of V3 can indeed produce an error in V3 - V4, which can cascade into the derivation of both E_X and E_Y in spacecraft coordinates. Moreover, the computation of the third component, E_Z , is reliant on E_X and E_Y via $\mathbf{E} \cdot \mathbf{B} = 0$. As a result, the error produced by this wake effect will strongly affect all three components of the electric field.

Additionally, the electric fields were rotated according to proton velocity measurements from SPC. Velocity moments from SPAN-ion were also examined, but also resulted in a 90° deviation from the model. However, it is possible that, within the Venusian magnetosheath, the full plasma distribution was not measured. SPC is directed sunward and

requires the core of the plasma distribution to be within 30° of its field-of-view (FOV) before the measurement degrades. Due to the orientation of the spacecraft, SPAN-ion was not pointed in the ram flow direction for the VGA1. The consequence is that only a partial distribution function of ions was measured, which affects and partially skews the derived plasma parameters. Velocities moments will inherently contain this offset if the core of the distribution is not in the FOV. Three-dimensional bi-maxwellians fits to the raw data can partially account for a part of this offset (Livi, private communication).

While the orientation of the observed electric field differs from those induced from the current vortex model by 90° , the spatial size, \mathbf{E} field amplitude, and induced $\Delta|\mathbf{B}|$ of the model are remarkably consistent with all observations. While the orientation of the electric field highlights specialized analysis is necessary during VGA1, there is sufficient evidence to support that these magnetic hole signatures are consistent with electron current vortices.

According to our analysis, a current vortex with an amplitude of 1.75 A/m^2 is required to induce the observed decrease in $|\mathbf{B}|$ shown in Figures 2 and 3. The electric fields seen with these $|\mathbf{B}|$ decreases suggest the current corresponds to electrons traveling at speeds on the order of 1000 km/s , up to 5 times faster than the observed proton velocity moments. Moreover, at least eleven sub-proton-scale magnetic holes were identified throughout PSP’s encounter with Venus. This suggests these structures are a common structure within the Venusian magnetosheath.

As stated previously, sub-proton-scale magnetic holes have arisen in multiple plasma turbulence simulations (Haynes et al., 2015; Roytershteyn et al., 2015). They have been suggested as a coherent structure that can arise naturally through turbulence. Observations in the terrestrial magnetosheath have also shown that sub-proton-scale magnetic holes can be seen with electron trapping (Huang et al., 2017) and electron heating perpendicular to the magnetic field (Liu et al., 2019). It is therefore possible that these structures may play a role or be a signature of turbulent dissipation. It is also possible they have evolved from other mechanisms (e.g. the mirror or tearing instability). What is clear, however, is the process that generates sub-proton-scale magnetic holes are present at both Earth and Venus.

6 Conclusion

On October 3rd, 2018, the Parker Solar Probe spacecraft encountered the Venusian magnetosheath as part of a gravity assist maneuver. During this encounter, localized depressions in magnetic field strength were observed with spatial scales less than the local thermal proton gyroradius, consistent with characteristics of sub-proton-scale magnetic holes. Eleven sub-proton-scale magnetic hole candidates were identified within the Venusian magnetosheath. No candidates were found in the solar wind during prior to the initial shock crossing.

Sub-proton-scale magnetic holes have been observed in many regions of the terrestrial magnetosphere with diverse plasma conditions. It is now clear, by additional reports of their presence at Venus, that they are indicative of a universal plasma process. Additionally, these observations, as well as the modeled comparison, suggest that the Venusian magnetosheath is host to widespread, large-amplitude, small-scale, electron current structures. It is unclear how such structures manifest or how they affect their plasma environment. Their importance to Venusian microphysics is consequently unclear. Understanding them, however, can lead to unprecedented insights to the microphysical processes that occur within the Venusian magnetosphere.

The Parker Solar Probe mission will engage in a total of seven flybys of Venus. These flybys cover multiple regions of the Venusian space plasma environment, including the bow shock, foreshock and magnetotail. With the advanced capabilities available on Parker Solar Probe, we stand to gain a better understanding of the microphysics that take place at Venus than we ever had and place those processes within the broader context of planetary electrodynamics across the inner solar system.

Acknowledgments

This work was made possible by the Parker Solar Probe mission. The FIELDS experiment on the Parker Solar Probe spacecraft was designed and developed under NASA contract NNN06AA01C. All data are available at <http://fields.ssl.berkeley.edu/>.

References

Ahmadi, N., Germaschewski, K., & Raeder, J. (2017). Simulation of magnetic holes formation in the magnetosheath. *Physics of Plasmas*, 24(12). Retrieved from

- 385 <http://dx.doi.org/10.1063/1.5003017> doi: 10.1063/1.5003017
- 386 Bale, S. D., Goetz, K., Harvey, P. R., Turin, P., Bonnell, J. W., de Wit, T., ...
- 387 Wygant, J. R. (2016, 12). The FIELDS Instrument Suite for Solar Probe Plus.
- 388 *Space Science Reviews*, 204(1), 49–82. Retrieved from [https://doi.org/](https://doi.org/10.1007/s11214-016-0244-5)
- 389 10.1007/s11214-016-0244-5 doi: 10.1007/s11214-016-0244-5
- 390 Balikhin, M. A., Pokhotelov, O. A., Walker, S. N., Boynton, R. J., & Beloff, N.
- 391 (2010). Mirror mode peaks: THEMIS observations versus theories. *Geophysical*
- 392 *Research Letters*, 37(5), n/a-n/a. doi: 10.1029/2009gl042090
- 393 Balikhin, M. A., Sibeck, D. G., Runov, A., & Walker, S. N. (2012). Mag-
- 394 netic holes in the vicinity of dipolarization fronts: Mirror or tearing struc-
- 395 tures? *Journal of Geophysical Research: Space Physics*, 117(8), 1–14. doi:
- 396 10.1029/2012JA017552
- 397 Califano, F., Hellinger, P., Kuznetsov, E., Passot, T., Sulem, P. L., & TráVn\`iĉEk,
- 398 P. M. (2008, 8). Nonlinear mirror mode dynamics: Simulations and mod-
- 399 eling. *Journal of Geophysical Research (Space Physics)*, 113, A08219. doi:
- 400 10.1029/2007JA012898
- 401 Case, A. W., Kasper, J. C., Stevens, M. L., Korreck, K. E., Paulson, K., Daigneau,
- 402 P., ... Martinović, M. M. (2020, 2). The Solar Probe Cup on the Parker
- 403 Solar Probe. *The Astrophysical Journal Supplement Series*, 246(2), 43.
- 404 Retrieved from <https://doi.org/10.3847/2F1538-4365%2Fab5a7b> doi:
- 405 10.3847/1538-4365/ab5a7b
- 406 Ergun, R. E., Carlson, C. W., Mc Fadden, J. P., Mozer, F. S., Muschietti, L., Roth,
- 407 I., & Strangeway, R. J. (1998, 7). Debye-scale plasma structures associated
- 408 with magnetic-field-aligned electric fields. *Physical Review Letters*, 81(4),
- 409 826–829. doi: 10.1103/PhysRevLett.81.826
- 410 Fox, N. J., Velli, M. C., Bale, S. D., Decker, R., Driesman, A., Howard, R. A., ...
- 411 Szabo, A. (2016, 12). The Solar Probe Plus Mission: Humanity’s First Visit
- 412 to Our Star. *Space Science Reviews*, 204(1), 7–48. Retrieved from [https://](https://doi.org/10.1007/s11214-015-0211-6)
- 413 doi.org/10.1007/s11214-015-0211-6 doi: 10.1007/s11214-015-0211-6
- 414 Ge, Y. S., McFadden, J. P., Raeder, J., Angelopoulos, V., Larson, D., & Constan-
- 415 tinescu, O. D. (2011, 1). Case studies of mirror-mode structures observed
- 416 by THEMIS in the near-Earth tail during substorms. *Journal of Geophysical*
- 417 *Research (Space Physics)*, 116, A01209. doi: 10.1029/2010JA015546

- 418 Gershman, D. J., Dorelli, J. C., Viñas, A. F., Avanov, L. A., Gliese, U., Barrie,
419 A. C., . . . Burch, J. L. (2016). Electron dynamics in a subproton-gyroscale
420 magnetic hole. *Geophysical Research Letters*. doi: 10.1002/2016GL068545
- 421 Goodrich, K. A., Ergun, R. E., & Stawarz, J. E. (2016). Electric fields associated
422 with small-scale magnetic holes in the plasma sheet: Evidence for electron
423 currents. *Geophysical Research Letters*. doi: 10.1002/2016GL069601
- 424 Goodrich, K. A., Ergun, R. E., Wilder, F. D., Burch, J., Torbert, R., Khotyaintsev,
425 Y., . . . Malaspina, D. M. (2016a). MMS Multipoint electric field observa-
426 tions of small-scale magnetic holes. *Geophysical Research Letters*, 43(12),
427 5953–5959. doi: 10.1002/2016GL069157
- 428 Goodrich, K. A., Ergun, R. E., Wilder, F. D., Burch, J., Torbert, R., Khotyaintsev,
429 Y., . . . Malaspina, D. M. (2016b). MMS Multipoint electric field obser-
430 vations of small-scale magnetic holes. *Geophysical Research Letters*. doi:
431 10.1002/2016GL069157
- 432 Halekas, J. S., Whittlesey, P., Larson, D. E., McGinnis, D., Maksimovic, M.,
433 Berthomier, M., . . . Harvey, P. R. (2020). Electrons in the Young Solar
434 Wind: First Results from the Parker Solar Probe. *The Astrophysical Journal*
435 *Supplement Series*, 246(2), 22. Retrieved from [http://dx.doi.org/10.3847/](http://dx.doi.org/10.3847/1538-4365/ab4cec)
436 1538-4365/ab4cec doi: 10.3847/1538-4365/ab4cec
- 437 Haynes, C. T., Burgess, D., Camporeale, E., & Sundberg, T. (2015, 1). Electron
438 vortex magnetic holes: A nonlinear coherent plasma structure. *Physics of Plas-*
439 *mas*, 22(1), 12309. doi: 10.1063/1.4906356
- 440 Huang, S. Y., Sahraoui, F., Yuan, Z. G., He, J. S., Zhao, J. S., Contel, O. L., . . .
441 Burch, J. L. (2017). Magnetospheric Multiscale Observations of Electron Vor-
442 tex Magnetic Hole in the Turbulent Magnetosheath Plasma. *The Astrophysical*
443 *Journal*, 836(2), L27. doi: 10.3847/2041-8213/aa5f50
- 444 Johnson, J. R., & Cheng, C. Z. (1997, 4). Global structure of mirror modes in the
445 magnetosheath. *Journal of Geophysical Research (Space Physics)*, 102, 7179–
446 7190. doi: 10.1029/96JA03949
- 447 Kasper, J. C., Abiad, R., Austin, G., Balat-Pichelin, M., Bale, S. D., Belcher,
448 J. W., . . . Zank, G. (2016, 12). Solar Wind Electrons Alphas and Protons
449 (SWEAP) Investigation: Design of the Solar Wind and Coronal Plasma In-
450 strument Suite for Solar Probe Plus. *Space Science Reviews*, 204(1), 131–

186. Retrieved from <https://doi.org/10.1007/s11214-015-0206-3> doi:
10.1007/s11214-015-0206-3
- Kuznetsov, E. A., Passot, T., & Sulem, P. L. (2008). Nonlinear theory of mirror
instability near its threshold. *JETP Letters*, 86(10), 637–642. doi: 10.1134/
S0021364007220055
- Liu, H., Zong, Q. G., Zhang, H., Xiao, C. J., Shi, Q. Q., Yao, S. T., ... Rankin,
R. (2019). MMS observations of electron scale magnetic cavity embedded
in proton scale magnetic cavity. *Nature Communications*, 10(1), 1–11. doi:
10.1038/s41467-019-08971-y
- Malaspina, D. M., Ergun, R. E., Bolton, M., Kien, M., Summers, D., Stevens, K., ...
Goetz, K. (2016). The Digital Fields Board for the FIELDs instrument suite
on the Solar Probe Plus mission: Analog and digital signal processing. *Journal*
of Geophysical Research: Space Physics. doi: 10.1002/2016JA022344
- Roytershteyn, V., Karimabadi, H., & Roberts, A. (2015). Generation of magnetic
holes in fully kinetic simulations of collisionless turbulence. *Philosophical*
Transactions of the Royal Society A: Mathematical, Physical and Engineering
Sciences, 373(2041), 1–13. doi: 10.1098/rsta.2014.0151
- Russell, C. T., Jian, L. K., Luhmann, J. G., Zhang, T. L., Neubauer, F. M., Skoug,
R. M., ... Cowee, M. M. (2008, 8). Mirror mode waves: Messengers from
the coronal heating region. *Geophysical Research Letters*, 35, L15101. doi:
10.1029/2008GL034096
- Soucek, J., Lucek, E., & Dandouras, I. (2008, 4). Properties of magnetosheath
mirror modes observed by Cluster and their response to changes in plasma
parameters. *Journal of Geophysical Research (Space Physics)*, 113, A04203.
doi: 10.1029/2007JA012649
- Southwood, D. J., & Kivelson, M. G. (1993). Mirror instability: 1. Physical mecha-
nism of linear instability. *Journal of Geophysical Research*, 98(A6), 9181. doi:
10.1029/92ja02837
- Stix, T. H. (1992). *Waves in plasmas*. AIP-Press.
- Sun, W. J., Shi, Q. Q., Fu, S. Y., Pu, Z. Y., Dunlop, M. W., Walsh, A. P.,
... Fazakerley, A. (2012, 3). Cluster and TC-1 observation of mag-
netic holes in the plasma sheet. *Annales Geophysicae*, 30, 583–595. doi:
10.5194/angeo-30-583-2012

- 484 Sundberg, T., Burgess, D., & Haynes, C. T. (2015, 4). Properties and ori-
 485 gin of subproton-scale magnetic holes in the terrestrial plasma sheet.
 486 *Journal of Geophysical Research (Space Physics)*, 120, 2600–2615. doi:
 487 10.1002/2014JA020856
- 488 Tenerani, A., Califano, F., Pegoraro, F., & Le Contel, O. (2012, 5). Coupling be-
 489 tween whistler waves and slow-mode solitary waves. *Physics of Plasmas*, 19(5),
 490 52103. doi: 10.1063/1.4717764
- 491 Tenerani, A., Contel, O. L., Califano, F., Robert, P., Fontaine, D., Cornilleau-
 492 Wehrlin, N., & Sauvaud, J.-A. (2013, 10). Cluster observations of whistler
 493 waves correlated with ion-scale magnetic structures during the 17 August
 494 2003 substorm event. *Journal of Geophysical Research (Space Physics)*, 118,
 495 6072–6089. doi: 10.1002/jgra.50562
- 496 Whittlesey, P. L., Larson, D. E., Kasper, J. C., Halekas, J., Abatcha, M., Abiad,
 497 R., ... Verniero, J. L. (2020). The Solar Probe ANalyzersElectrons on the
 498 Parker Solar Probe . *The Astrophysical Journal Supplement Series*, 246(2),
 499 74. Retrieved from <http://dx.doi.org/10.3847/1538-4365/ab7370> doi:
 500 10.3847/1538-4365/ab7370
- 501 Wintertialter, D., Neugebauer, M., Goldstein, B. E., Smith, E. J., Bame, S. J., &
 502 Balogh, A. (1994). Ulysses field and plasma observations of magnetic holes
 503 in the solar wind and their relation to mirror-mode structures. *Journal of*
 504 *Geophysical Research: Space Physics*. doi: 10.1029/94JA01977
- 505 Yao, S. T., Wang, X. G., Shi, Q. Q., Pitkänen, T., Hamrin, M., Yao, Z. H., ... Liu,
 506 J. (2017). Observations of kinetic-size magnetic holes in the magnetosheath.
 507 *Journal of Geophysical Research: Space Physics*, 122(2), 1990–2000. doi:
 508 10.1002/2016JA023858

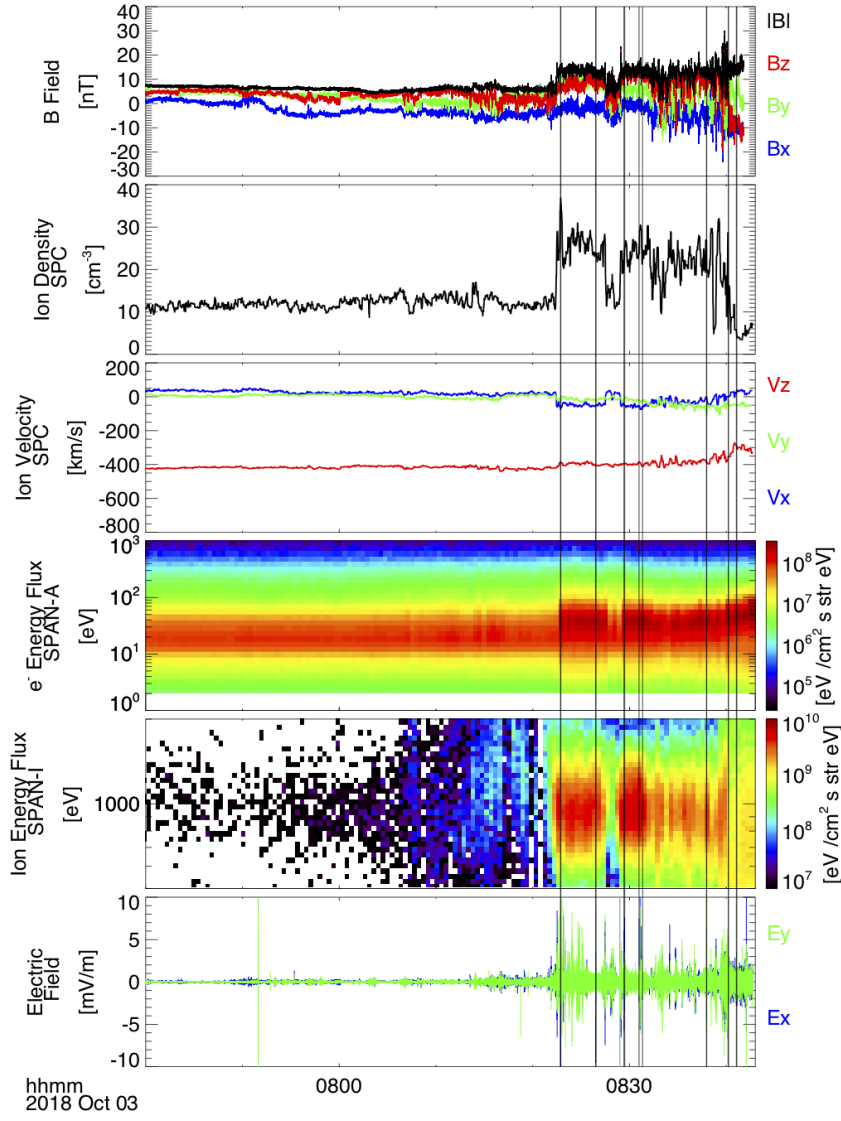


Figure 1. Overview of the first Venus Flyby undertaken by Parker Solar Probe. The plot shows, in descending order, magnetic field, proton density from SPC, proton velocity from SPC, electron energy flux, proton energy flux from SPAN-ion, and electric field. All vectors are in spacecraft coordinates. The Parker spacecraft initially measured solar wind before encountering the Venusian shock at $\sim 08:22:20$ UTC. It then observed the Venusian magnetosheath as well as other bow shock crossings before the end of the encounter at $\sim 08:50$. All vertical lines mark times in which sub-proton-scale magnetic holes were observed.

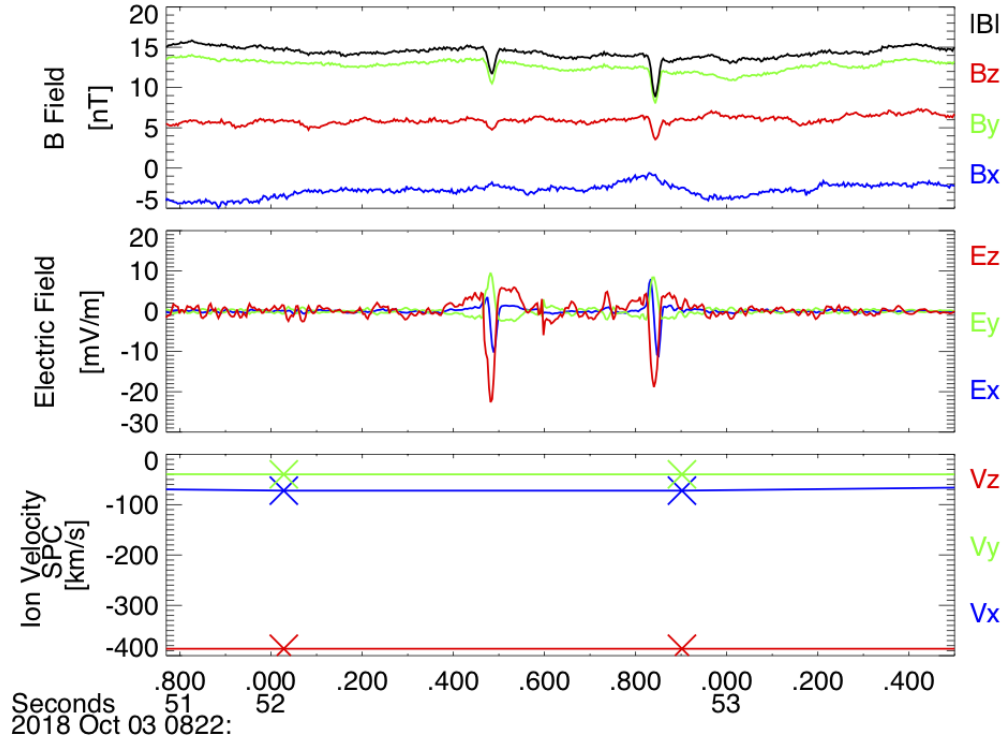


Figure 2. Two example magnetic hole candidates. This figure shows a 1.6 second zoomed in view of the magnetic field, electric field, and proton velocity at ~08:22:52 UTC, approximately 30 seconds after Parker Solar Probe made its initial Venusian bow shock crossing. Bipolar and unipolar electric field signatures are observed in tandem with localized (50 ms) depressions in magnetic field strength.

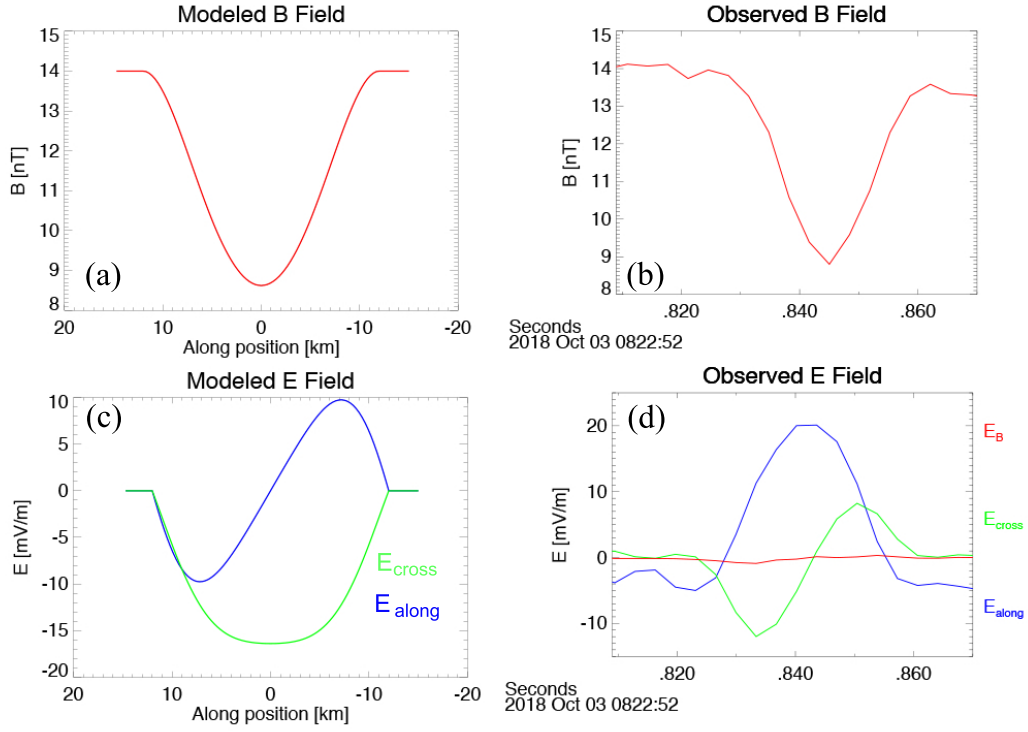
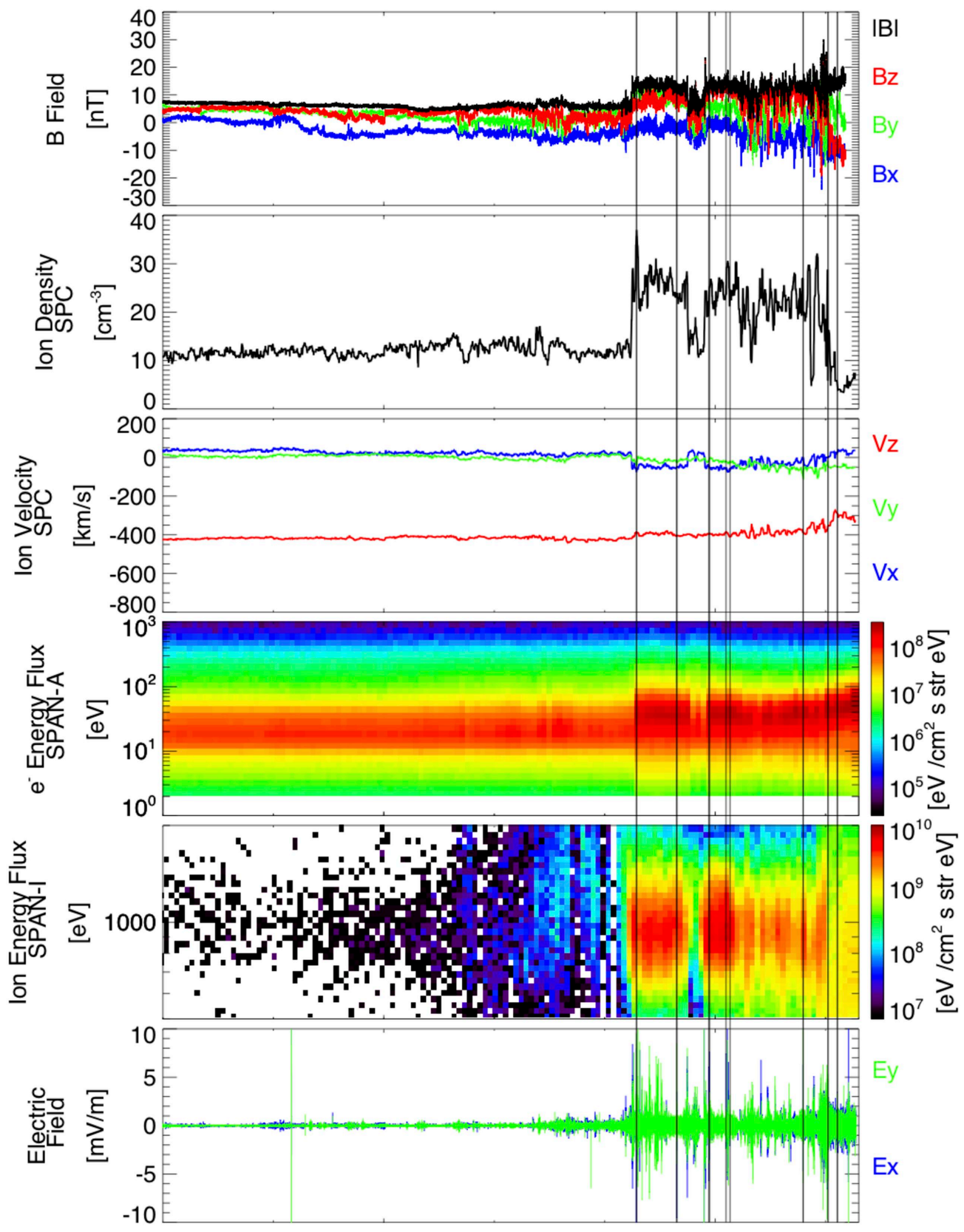


Figure 3. This figure shows a direct comparison between magnetic (a) and electric (c) field from the modeled electron vortex and the magnetic (b) and electric (d) field observed by Parker in the Venusian magnetosheath. The observed magnetic and electric field were transformed into the local plasma frame.

Figure 1.



hhmm
2018 Oct 03

Figure 2.

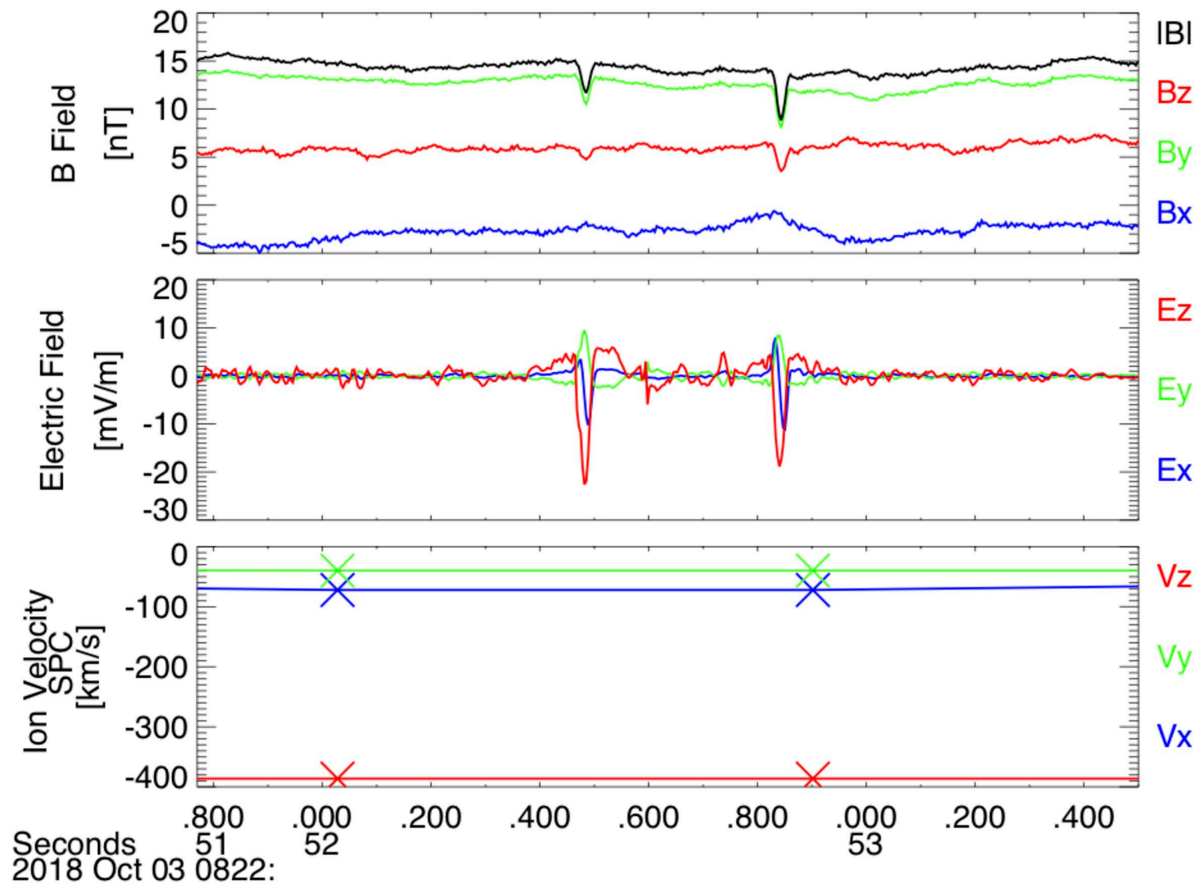
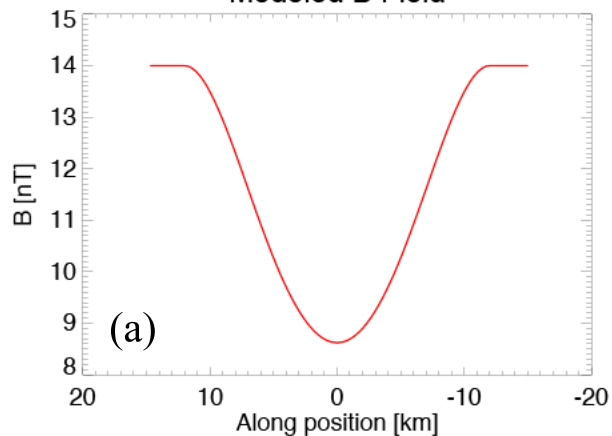
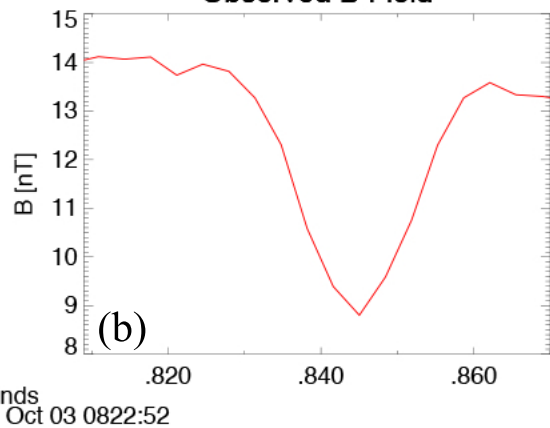


Figure 3.

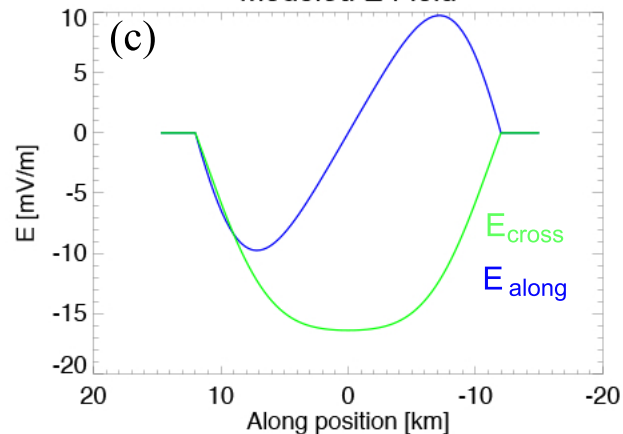
Modeled B Field



Observed B Field



Modeled E Field



Observed E Field

